

Comparison of aerosol optical properties and water vapor among ground and airborne lidars and Sun photometers during TARFOX

R. Ferrare,¹ S. Ismail,¹ E. Browell,¹ V. Brackett,² M. Clayton,² S. Kooi,² S. H. Melfi,³ D. Whiteman,⁴ G. Schwemmer,⁴ K. Evans,³ P. Russell,⁵ J. Livingston,⁶ B. Schmid,⁷ B. Holben,⁴ L. Remer,⁴ A. Smirnov,⁸ and P. V. Hobbs⁹

Abstract. We compare aerosol optical thickness (AOT) and precipitable water vapor (PWV) measurements derived from ground and airborne lidars and Sun photometers during the Tropospheric Aerosol Radiative Forcing Observational Experiment. Such comparisons are important to verify the consistency between various remote sensing measurements before employing them in any assessment of the impact of aerosols on the global radiation balance. Total scattering ratio and extinction profiles measured by the ground-based NASA Goddard Space Flight Center scanning Raman lidar system, which operated from Wallops Island, Virginia (37.86°N, 75.51°W), are compared with those measured by the Lidar Atmospheric Sensing Experiment (LASE) airborne lidar system aboard the NASA ER-2 aircraft. Bias and root-mean-square differences indicate that these measurements generally agreed within about 10%. Aerosol extinction profiles and estimates of AOT are derived from both lidar measurements using a value for the aerosol extinction/backscattering ratio $S_a = 60$ sr for the aerosol extinction/backscattering ratio, which was determined from the Raman lidar measurements. The lidar measurements of AOT are found to be generally within 25% of the AOT measured by the NASA Ames Airborne Tracking Sun Photometer (AATS-6). However, during certain periods the lidar and Sun photometer measurements of AOT differed significantly, possibly because of variations in the aerosol physical characteristics (e.g., size, composition) which affect S_a . Estimates of PWV, derived from water vapor mixing ratio profiles measured by LASE, are within 5–10% of PWV derived from the airborne Sun photometer. Aerosol extinction profiles measured by both lidars show that aerosols were generally concentrated in the lowest 2–3 km.

1. Introduction

Accurate aerosol measurements are required for understanding shortwave (visible) radiative transfer and the factors controlling the Earth's climate, since aerosols scatter and absorb solar radiation and alter the structure of clouds. By reflecting solar radiation, atmospheric aerosols may reduce the warming associated with increases in greenhouse gases [Charlson *et al.*, 1992; Intergovernmental Panel on Climate Change (IPCC), 1995], although the magnitude of this direct aerosol radiative cooling effect may be small [Kiehl and Briegleb, 1993; IPCC, 1996] or even negligible [Hansen *et al.*, 1997]. Because of their short lifetime in the troposphere, aerosols have large spatial and temporal variabilities, so that it is difficult to accurately assess their direct and in-

direct effects on clouds. These variabilities, along with uncertainties in the physical and optical properties of aerosols, lead to the result that aerosols are one of the largest single uncertainties in computing the net radiative forcing due to anthropogenic changes in the chemical composition of the atmosphere and their resulting effects on climate change [IPCC, 1996; Schwartz and Andreae, 1996].

The Tropospheric Aerosol Radiative Forcing Observational Experiment (TARFOX) intensive field campaign, which was conducted off the east coast of the United States between July 10 and 31, 1996, was designed to reduce uncertainties in estimates of the effects of anthropogenic aerosols on climate by measuring the direct radiative effects and the optical, physical, and chemical properties of aerosols [Russell *et al.*, 1999a]. Ground, aircraft, and satellite-based sensors measured the sensitivity of radiative fields at various atmospheric levels to aerosol optical properties (i.e., optical thickness, phase function, single-scattering albedo) and to the vertical profile of aerosols. One of the principal goals was to perform a series of "column-closure" studies by using the degree of closure (i.e., consistency) among different measurements and analyses of aerosol properties to assess (and potentially reduce) uncertainties in predicted aerosol climate forcing. These include both "internal closure" and "external closure" studies. "Internal closure" is assessed by comparing aerosol optical properties (e.g., extinction, single-scattering albedo, asymmetry parameter) with those derived from simultaneous measurements of the aerosol physical characteristics (i.e., size and composition). "External closure" is assessed by comparing aero-

¹NASA Langley Research Center, Hampton, Virginia.

²SAIC/NASA Langley Research Center, Hampton, Virginia.

³University of Maryland Baltimore County, Baltimore, Maryland.

⁴NASA Goddard Space Flight Center, Greenbelt, Maryland.

⁵NASA Ames Research Center, Moffett Field, California.

⁶SRI International, Menlo Park, California.

⁷BAER Institute, San Francisco, California.

⁸SSAI/NASA Goddard Space Flight Center, Greenbelt, Maryland.

⁹Department of Atmospheric Science, University of Washington, Seattle, Washington.

sol optical properties, namely aerosol extinction and optical depth, derived from various methods, including surface- and aircraft-based transmission measurements, in situ measurements on aircraft, satellite measurements of scattered solar radiation, and ground- and aircraft-based lidars.

The use of lidar aerosol profiles acquired during TARFOX for internal closure studies is discussed by *Redemann et al.* [this issue]. In this paper we use aerosol profiles measured by two lidar systems to perform a series of external closure studies. The two lidars are the ground-based NASA/Goddard Space Flight Center (GSFC) scanning Raman lidar (SRL) and the airborne Lidar Atmospheric Sensing Experiment (LASE) system. The SRL, which was located at NASA Wallops Flight Facility (37.86°N, 75.51°W) approximately 3.5 km from the coast, measured profiles of aerosol backscattering during TARFOX. The lidar measurements were also used to derive the aerosol extinction/backscattering ratio (S_a). LASE flew on the NASA ER-2 aircraft and measured vertical profiles of total backscatter and water vapor density during a series of nine flights. From these we derive total scattering ratio and water vapor mixing ratio profiles. Using the S_a value derived from the Raman lidar measurements, we use both lidar data sets to derive aerosol extinction profiles. Using these profiles, we derive estimates of aerosol optical thickness (AOT) and compare these with AOT measurements from both ground and airborne Sun photometers. In a separate paper [*Ferrare et al.*, this issue] we compare the AOT derived from the airborne LASE measurements with AOT derived from the Moderate Resolution Imaging Spectroradiometer (MODIS) airborne simulator and the ATSR-2 (Along Track and Scanning Radiometer 2) sensor on the ERS-2 (European Remote Sensing Satellite 2), and the LASE aerosol extinction profiles with extinction profiles derived from in situ airborne measurements.

We also compute precipitable water vapor (PWV) as a function of altitude from the LASE measurements and compare these with PWV derived from the Sun photometer measurements. Since Sun photometers are being used to measure precipitable water vapor for studying atmospheric processes and will be used for validation of satellite PWV measurements [*King et al.*, 1999], we took advantage of the coincident LASE and Sun photometer measurements acquired during TARFOX to compare PWV measured by these remote sensors. Previous ground-based measurements have also shown that PWV and AOT are often highly correlated [*Ferrare et al.*, 1998a, this issue].

2. NASA GSFC Scanning Raman Lidar

The GSFC scanning Raman lidar employs two different lasers depending on whether data are acquired at nighttime or daytime. For nighttime operations the system uses a XeF excimer laser that transmits light at 351 nm. Detailed descriptions of the use of this laser to measure water vapor and aerosols during nighttime operations are given by *Ferrare et al.* [1995], *Whiteman et al.* [1998], and *Ferrare et al.* [1998a, b].

In the spring of 1996 the instrument was modified to acquire aerosol and water vapor profiles during daytime operations. The addition of a Nd:YAG laser and the incorporation of a narrow-band, narrow field-of-view system helped facilitate daytime measurements of aerosols and water vapor. During TARFOX, where these daytime modifications were used for the first time, the Nd:YAG operated at 30 Hz with an average power of 5 W. Light backscattered by molecules and aerosols at the laser wavelength as well as Raman-scattered light from water vapor

(408 nm) and nitrogen (387 nm) molecules is collected by a 0.76 m, F5.2, variable field-of-view (.5 - 3.0 rad) Dall-Kirkham telescope, which is mounted horizontally on a 3.7 m optical table. The telescope is aligned with a large (1.2m × 0.8m) flat mirror, which is also mounted on the optical table. During these operations the optical table slid through an opening in the back of the trailer deploying the scan mirror that has a 180° horizon-to-horizon scan capability. Using the motorized scan mirror, atmospheric profiles can be acquired at any angle in a single plane perpendicular to the trailer or continuously scanned from horizon to horizon.

Two channels, operating in the photon counting mode, are employed for each wavelength to measure signals throughout the troposphere and lower stratosphere. A beam splitter directs 5% of the return signals into the low-sensitivity channels and about 95% into the high-sensitivity channels. While the low-sensitivity channels employed a wide (2 mrad) field of view, the high-sensitivity channels used a narrow (0.3 mrad) field of view to reduce the background skylight and increase the signal-to-noise ratio of the lidar measurements. In normal operation, data are recorded as 1 min profiles corresponding to the accumulation of signals from about 1740 laser shots. The photon counting data have a range resolution of 75 m. Several analysis programs operate in real time to monitor system performance and to provide real-time images of the evolution of both aerosols and water vapor.

Unlike most lidars that measure only the signal elastically backscattered by molecules and aerosols, Raman lidar is also used to simultaneously measure inelastic molecular scattering to directly compute the aerosol extinction cross section since aerosol extinction, and not aerosol backscatter, affects the Raman signals [*Ansmann et al.*, 1990]. The total extinction, because of both scattering and absorption by molecules and aerosols, is found from the derivative of the logarithm of the nitrogen Raman return signal. Aerosol extinction is then found by subtracting molecular extinction, which is computed using coincident radiosonde density measurements. *Ferrare et al.* [1998a] describe the methods used to compute aerosol extinction profiles using the scan data from the SRL.

The aerosol scattering ratio, which is defined as the ratio of the total (aerosol plus molecular) scattering to molecular scattering, is computed directly from the lidar data. Molecular backscattering is measured using the Raman nitrogen return, while the combined aerosol plus molecular backscattering is measured using the return signal at the laser wavelength. The aerosol volume backscatter cross section is computed from the scattering ratio and the molecular backscattering cross section, which is derived from the coincident radiosonde pressure and temperature profiles. Details of these aerosol algorithms are given by *Ferrare et al.* [1992, 1998a] and *Whiteman et al.* [1992].

Unfortunately, problems with the narrow field-of-view detector optics, coupled with low laser power, resulted in low signal-to-noise ratios in the Raman channels during daytime operations in TARFOX. (Improvements made to the system after TARFOX now permit the retrieval of both water vapor and aerosol extinction during daytime operations.) These low signal-to-noise ratios prevented daytime measurements of water vapor and restricted the use of the Raman nitrogen channel for computing aerosol extinction. During most of the daytime operations in TARFOX, aerosol extinction was computed by inverting the Rayleigh/Mie return signal at 351 nm following the method described by *Fernald* [1984]. This method requires an estimate of the aerosol extinction/backscattering ratio (S_a). Therefore using the methods

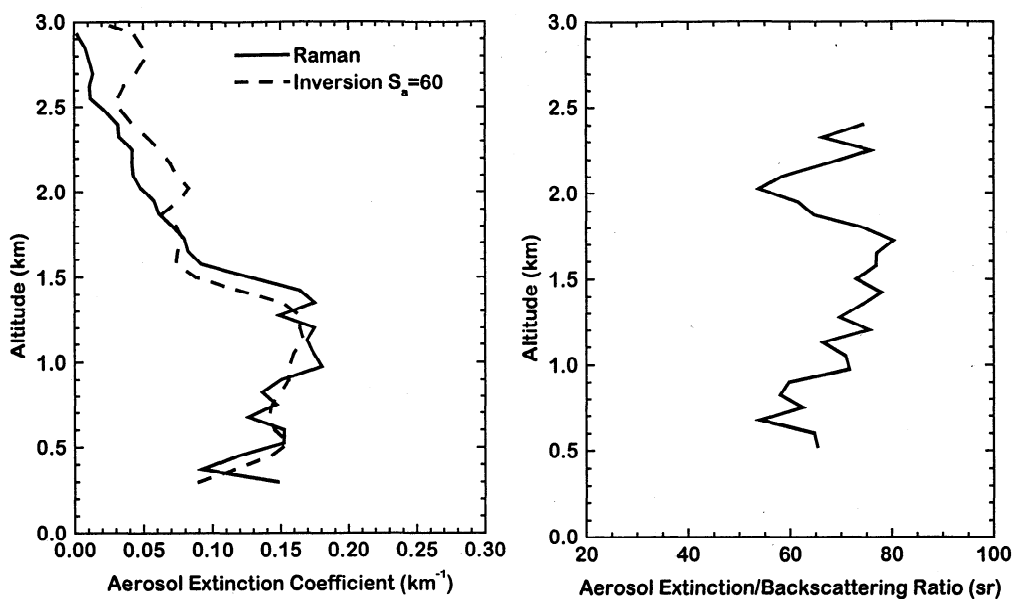


Figure 1. (left) Comparison of aerosol extinction profiles derived from Raman nitrogen channel (387 nm) and by inverting the signal at the laser wavelength (35 nm). (right) Aerosol extinction/backscatter ratio S_a derived on July 27, 1996.

described by Ferrare *et al.* [1998a], this ratio was derived using Raman nitrogen channel data acquired about 1 hour before sunset when solar background levels were low. These scan data were acquired between 2300 UTC July 27 and 0000 UTC on July 28 (1900-2000 EDT, July 27). Data acquired at scan angle angles of 0° (vertical), 55°, 75°, and 86° were used to construct composite aerosol extinction profiles. For the data acquired on July 27 an average value of $S_a = 60$ sr was determined from the simultaneous measurements of aerosol extinction and backscattering. This value also gave the best agreement between the aerosol extinction profile derived from the Raman nitrogen data and the aerosol extinction profiles obtained by inverting the return signal at the laser wavelength following the methods described by Ferrare *et al.* [1998a]. Figure 1 (left) shows a comparison of the aerosol extinction profiles derived from both methods and Figure 1(right)

shows the S_a profile derived from the Raman lidar measurements. On the basis of these results a value of $S_a = 60 \pm 10$ sr was used for the subsequent analyses.

At the lidar wavelength of 355 nm, effects of variations in S_a on the aerosol extinction profile depend on altitude, so increasing the value of S_a may either raise or lower the value of aerosol extinction. Figure 2 (left) shows a comparison of aerosol extinction profiles derived for various values of S_a . Although S_a varies with changes in the aerosol size distribution and composition [Evans, 1988; Ackermann, 1998], a constant value was used because of the lack of suitable Raman nitrogen measurements to evaluate this ratio on a daily basis. Previous studies have indicated that using a single value of S_a for retrievals of aerosol extinction profiles can lead to erroneous results [Ansmann *et al.*, 1992; Kunz and de Leeuw, 1993; Ferrare *et al.*, 1998a]. One of the objec-

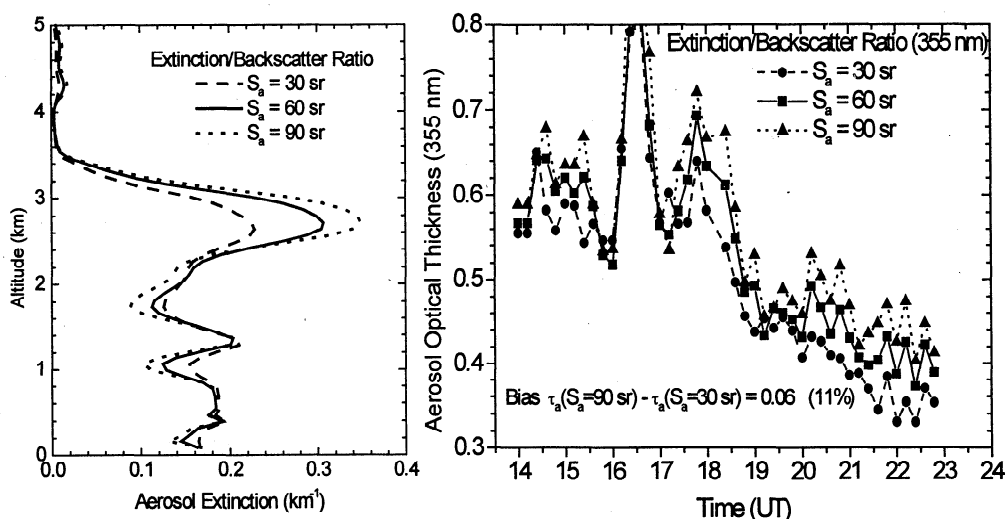


Figure 2. (left) Comparison of aerosol extinction profiles derived from Goddard Space Flight Center (GSFC) lidar data on July 27, 1996, using various values of the aerosol extinction/backscatter ratio. (right) Time series of aerosol optical thickness (AOT) derived from GSFC lidar aerosol extinction profiles showing sensitivity of AOT to S_a .

tives of this study was to determine, for a limited duration field experiment, the impact of using a single value of S_a on the determination of aerosol extinction profiles and, in turn, on the AOT derived from these profiles. The extensive suite of instruments that measured both aerosol scattering and AOT during TARFOX provided an opportunity to assess these lidar profiles.

Aerosol optical thickness (AOT) was derived during cloud-free periods by integrating the aerosol extinction profiles between altitudes of 0.020 and 5 km. On the basis of Raman lidar and LASE measurements discussed in section 7, the AOT, due to aerosols in the troposphere above 5 km, was less than 0.01. The estimated AOT at 355 nm due to stratospheric aerosols is approximately 0.01 during July 1996 [Jäger *et al.*, 1997]. The sensitivity of the total AOT across the troposphere to the value of S_a used in deriving the aerosol extinction profile by inverting the lidar data is shown in Figure 2 (right). Ferrare *et al.* [1998a] show that S_a can vary significantly with altitude and from day to day and that S_a varied from about 30 to 90 sr at a continental site in the United States. AOT increased by an average of about 0.06 (11%) when S_a increased from 30 to 90 sr, although differences in the derived AOT using these extreme S_a values can be as high as 50%. Using aerosol size distributions measured by in situ instrumentation on the University of Washington C-131A aircraft, J. P. Redemann (private communication, 1999) estimated layer-averaged values of $S_a = 82$ and 75 sr (at 355 nm) for July 17 and July 24, respectively. Aerosol size distributions derived from Cimel Sun photometer measurements were also used to estimate S_a during TARFOX (O. Dubovik, private communication, 1999).

These retrievals also gave an average value of $S_a = 75$ sr at 355 nm. Although the value of $S_a = 60 \pm 10$ sr derived from the SRL measurements on July 27 is slightly smaller than these estimates, the AOT retrieved using $S_a = 60$ sr should be generally within 10% of the AOT values derived using these higher S_a estimates, as shown in Figure 2 (right).

The SRL measurements were also used to determine the presence of clouds and to locate cloud base. The total scattering ratio profiles derived from the SRL data were examined for periods when the total scattering ratio exceeded 2.5 (at 355 nm). In a series of preliminary tests, cloud base altitudes determined using this technique were found to agree well with those measured by a micropulse lidar (MPL) and a Belfort laser ceilometer system [Demoz *et al.*, 1999]. The SRL measurements were used to identify clouds below an altitude of 12 km.

3. SRL Operations During TARFOX

During TARFOX the SRL was located at NASA Wallops Flight Facility approximately 3.5 km west of the coast. NASA/GSFC/Wallops Flight Facility (WFF) personnel launched radiosondes each day from a coastal site approximately 3 km down-range from the lidar. These radiosondes were typically launched at 1400 and 1830 UTC (1000 and 1430 EDT) each day. The lidar was oriented to acquire scan data both over this launch site and the land-ocean interface. Lidar operations began on July 10 but were interrupted for 5 days because of evacuation procedures associated with Hurricane Bertha. SRL operations resumed on

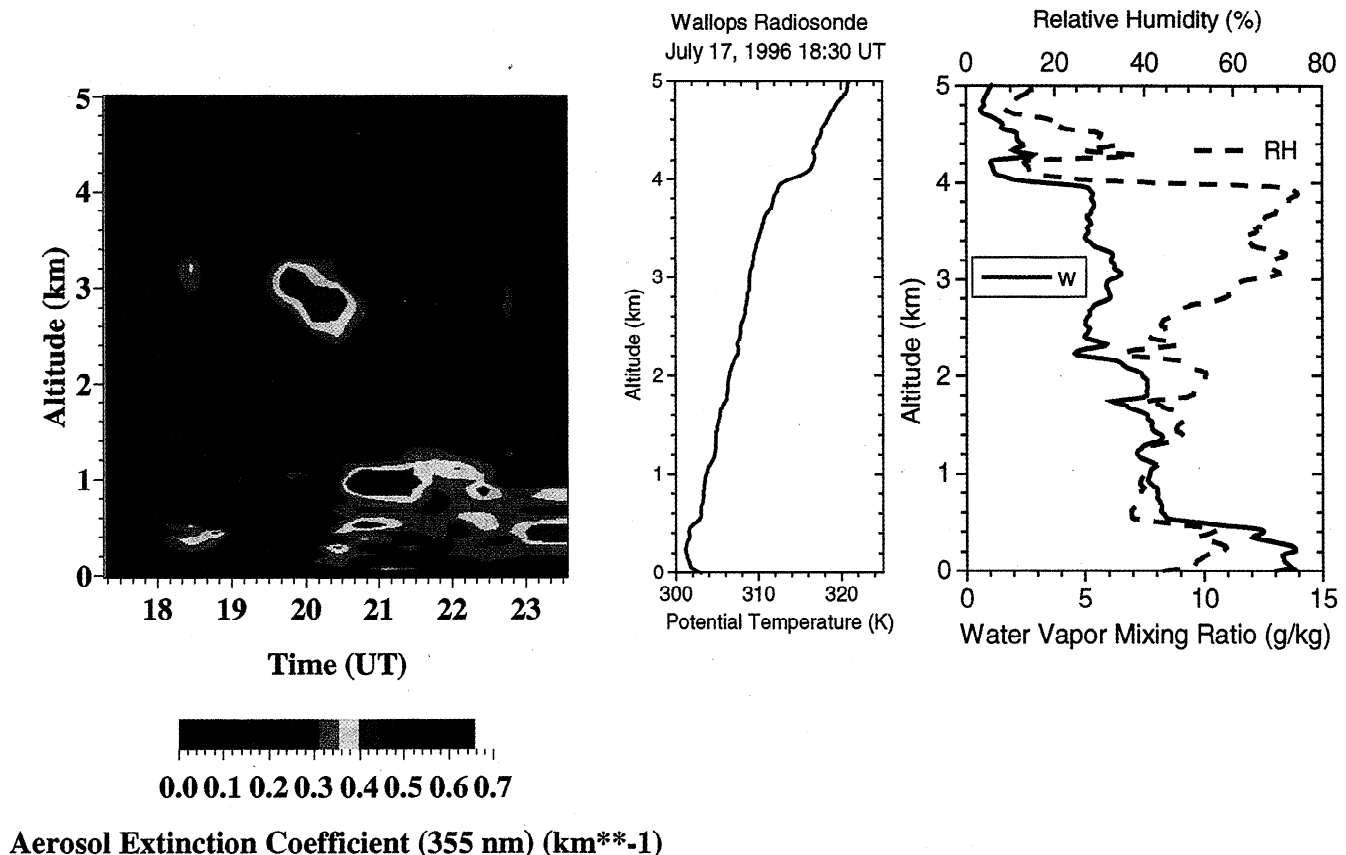


Plate 1. (left) Color image showing aerosol extinction profiles derived from GSFC lidar data during July 27, 1996. (right) Potential temperature, water vapor mixing ratio, and relative humidity profiles measured by a radiosonde launched from Wallops Island at 1830 UT on July 27.

July 16 and continued through July 31. The SRL operated for a total of 15 days and acquired approximately 95 hours of data.

4. GSFC SRL Aerosol Extinction Measurements

Aerosol extinction profiles were derived from the Raman lidar measurements for each day of operation. An example of aerosol extinction profiles derived for July 17 is shown in Plate 1 (left). During this day the SRL acquired data at four scan angles: 0°, 70°, 80°, and 86° measured from the zenith. Because vertical profiles were acquired 3 times as often as the other angles, nine consecutive vertical profiles were averaged together, while three consecutive profiles at each angle were averaged to reduce the random error in the data. Thus the data from each angle has an effective temporal resolution of 18 min. The resulting profiles at the three scan angles are combined to form profiles extending to within about 15 m of the surface. The temperature and density profiles measured by radiosondes typically launched at 1400 and 1830 UTC (1000 and 1430 EDT) were used to derive the molecular scattering profiles used in determining aerosol extinction profiles.

The aerosol extinction profiles shown in Plate 1 indicate that the highest aerosol extinction values were located near the top of the convective mixed layer. The potential temperature, water vapor mixing ratio, and relative humidity profiles measured by a radiosonde launched at Wallops Island at 1830 UTC are shown in Plate 1 (right). The lidar data indicate that the altitude of the convective mixed layer varied between 500 and 600 m until about 1930 UTC, when the layer rose to about 1.6 km. Note the rapid decrease in water vapor mixing ratio and relative humidity above this layer. The presence of an elevated aerosol layer between about 2.4 to 3.4 km in the lidar data is also correlated with the layer of increased relative humidity. During TARFOX the addition of water to aerosols in regions of high relative humidity significantly increases aerosol scattering when com-

pared to aerosol scattering produced by dry aerosols [Hegg et al., 1997; Kotchenruther et al., 1999].

5. SRL and Sun Photometer Aerosol Optical Thickness Comparison

During cloud-free periods, AOT derived from the lidar measurements were compared with those measured by ground and aircraft-based Sun photometers. A Cimel multiband automatic Sun- and sky-scanning radiometer [Holben et al., 1994; 1998] was deployed at a coastal site approximately 3 km east of the SRL. During TARFOX this sensor acquired aerosol measurements at 340, 380, 441, 672, 873, and 1022 nm during cloud-free periods. Aerosol optical thickness, phase function, size distribution, and integrated water vapor were derived from a combination of Sun and sky brightness measurements acquired by this instrument [Remer et al., 1997, 1999; Smirnov et al., 1999]. On the basis of intercomparisons with a reference Sun photometer at GSFC, which was calibrated using a series of spectral “Langley” plot data acquired at Mauna Loa, Hawaii, the resulting total error in the AOT at 340 nm is about 0.02 [Holben et al., 1998]. Using the methods described by Russell et al. [1993], AOT at 380, 451, 525, and 1021 nm were also derived using measurements acquired by the six-channel Ames Airborne Tracking Sun photometer (AATS-6) [Matsumoto et al., 1987] flown on the University of Washington C-131A. Hobbs [1999] gives a description of the entire aerosol and cloud sensing instrumentation on the University of Washington C-131A research aircraft. Russell et al. [1999b] show examples of optical depths and uncertainties derived from AATS 6 during TARFOX. The uncertainties, computed using equation (A22a) of Russell et al. [1993], include uncertainties in detector signal, instrument calibration, air mass, Rayleigh, ozone, and nitrogen dioxide optical depths and in diffuse light entering the Sun photometer. As shown in Plate 1

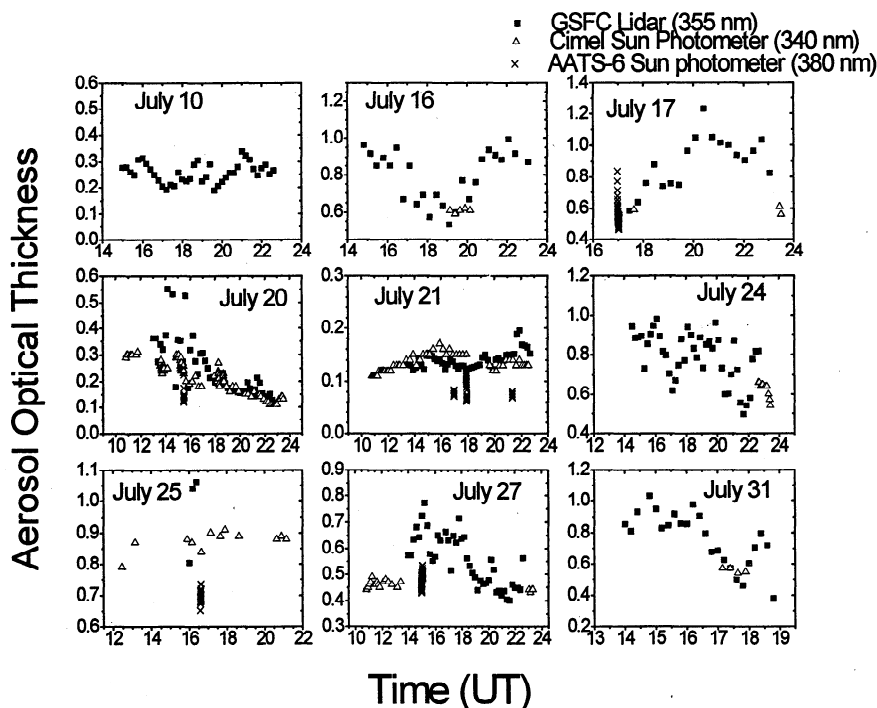


Figure 3. Time series showing AOT measured by GSFC lidar, ground-based Sun photometer, and AATS-6 airborne Sun photometer over Wallops Island during Tropospheric Aerosol Radiative Forcing Observational Experiment (TARFOX).

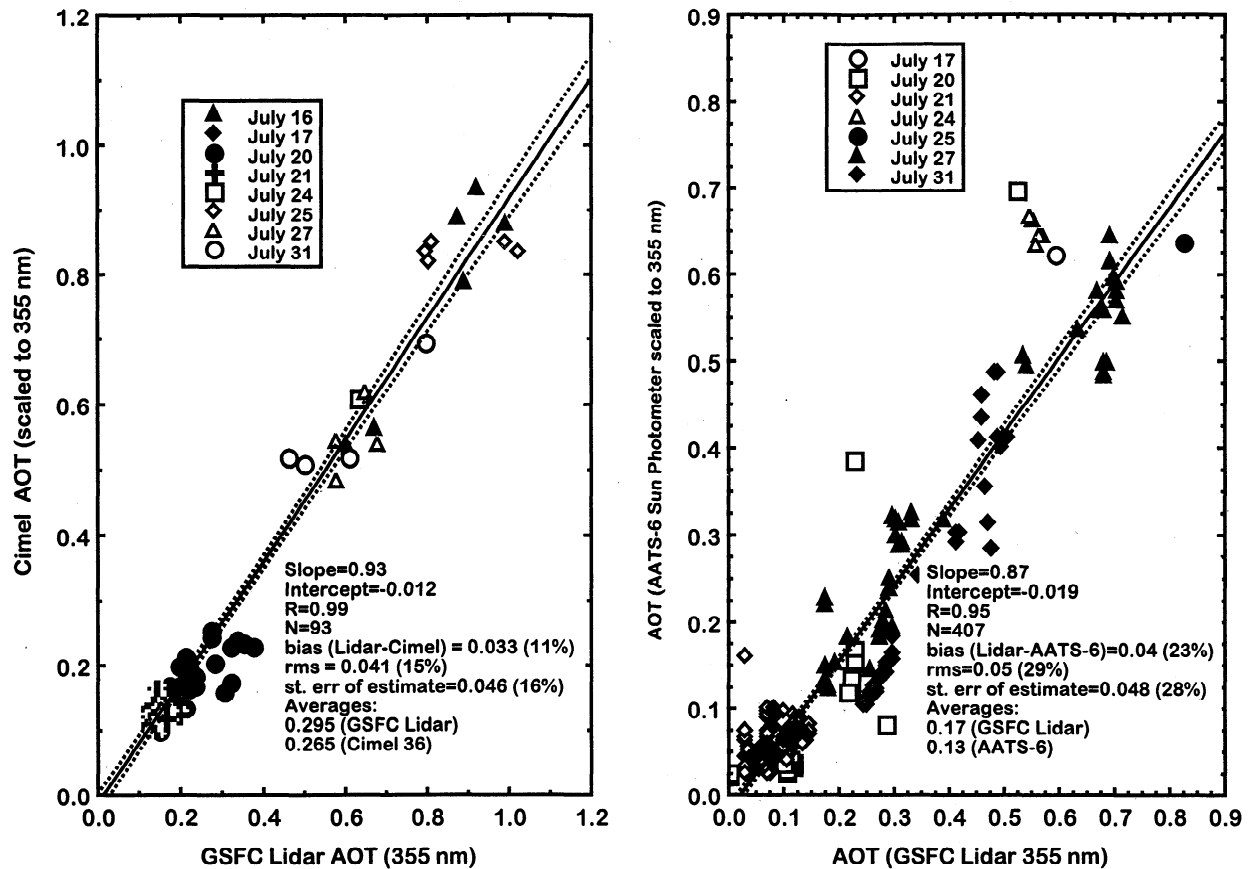


Figure 4. (left) Comparison of AOT measured by the GSFC lidar and Cimel Sun photometer during TARFOX. (right) Same except for AATS-6 airborne Sun photometer flown on the University of Washington (UW) C-131A aircraft. Linear least squares regression and corresponding 95% confidence bands are shown by the solid and dashed lines, respectively.

by Russell *et al.* [1999b], AATS-6 aerosol optical depth uncertainties were typically 0.01 (1σ) for the conditions of the TARFOX measurements.

Figure 3 shows a time series of the AOT derived from the SRL and the two Sun photometers. The AOT shown in Figure 3 represents values at the surface for the SRL and the Cimel Sun photometer, while the airborne Sun photometer data were acquired when the C-131A flew within about 100 m of the surface and within about 25 km of the lidar site. As discussed above, the paucity of ground-based Sun photometer measurements compared to the lidar measurements was due to the presence of clouds. Recall that the lidar values represent the AOT integrated between 0 and 5 km. The wide range of AOT shows the variety of aerosol conditions that were sampled, as the AOT varied between about 1.0, on July 16, 17, 24, 25, and 31, and about 0.1 on July 20 and 21. The decrease in AOT on July 20 was associated with the passage of an unusually strong cold front that passed over the eastern United States. Figure 3 shows that the AOT measured by the SRL and the ground-based Sun photometer were in general agreement. A more detailed comparison of AOT measurements is shown in Figure 4. Figure 4 (left) shows the comparison of the SRL AOT with the ground-based Cimel measurements, while Figure 4 (right) shows the comparison of the lidar values with the airborne Sun photometer measurements. In Figure 4 (left), the wavelength dependence of AOT measured by the CIMEL Sun photometer was interpolated using the Cimel

340 and 380 nm measurements to the 355 nm laser wavelength. When compared to the Cimel results, the SRL AOT measurements had a bias difference (SRL-Cimel) of 0.033 (11%) and a root-mean-square (rms) difference of 0.041 (15%). The reason for this difference is not clear. While part of this difference may be due to the use of a single S_a value to determine aerosol extinction and AOT from the lidar data, this reason probably cannot explain the entire difference. Recall from Figure 2 that relatively large ($S_a = 90$ to 30 sr) variations in the aerosol extinction/backscatter ratio produced rather small (11%) variations in the overall average AOT integrated from the lidar aerosol extinction measurements.

Figure 4 (right) shows a comparison of the AOT measured by the SRL and the airborne Sun photometer on the C-131A. In this case, AOT was computed as a function of altitude for the lidar data by integrating the aerosol extinction profiles between the top of the profile (about 12 km) and the C-131A aircraft altitude. Airborne Sun photometer data that were within 100 m in altitude and 25 km in horizontal distance were selected for this comparison. The airborne Sun photometer data were extrapolated from 380 nm to the lidar wavelength of 355 nm using the AOT wavelength dependence measured by the Cimel Sun photometer. When compared to the airborne Sun photometer AOT results, the AOT measured by the SRL had a bias difference (SRL-Sun photometer) of 0.04 (23%) and a rms difference of 0.05 (29%). This difference did not vary appreciably as a function of altitude.

6. LASE System

The Lidar Atmospheric Sensing Experiment (LASE) instrument was designed to provide high-resolution profiles of water vapor from the surface to tropopause level and columnar amounts of water vapor [Browell and Ismail, 1995; Browell et al., 1997; Moore et al., 1997]. LASE also provides simultaneous measurements of aerosol profiles in the troposphere and lower stratosphere during both daytime and nighttime operations.

A detailed description of the LASE system is given by Moore et al. [1997], so only a brief description will be given here. The laser system of LASE consists of a double-pulsed Ti:sapphire laser that operates in the 815-nm absorption band of water vapor and is pumped by a frequency-doubled flashlamp-pumped Nd:YAG laser. The wavelength of the Ti:sapphire laser is controlled by injection seeding with a diode laser that is frequency locked to a water vapor line using an absorption cell. LASE operates by locking to a strong water vapor line and electronically tuning to any spectral position on the absorption line to choose the suitable absorption cross section for optimum measurements over a range of water vapor concentrations in the atmosphere. LASE operated by alternating between strong (line center) and weak (side of strong line) water vapor cross sections for the on-line DIAL wavelength to measure water vapor throughout the troposphere. In addition, LASE can operate over two or three water vapor concentration regions to cover a large altitude region in the troposphere. This unique method of operation permits rapid and flexible absorption cross-section selection capability for water vapor measurements over the entire troposphere in a single pass. The LASE detector system consists of two silicon avalanche photodiodes (Si:APD), three digitizers to cover a large signal dynamic range (10^6), and a signal processor system designed to be relatively insensitive to rapid changes in signal levels. Comparisons of water vapor measurements made by airborne dew point and frost point hygrometers, NASA GSFC Raman lidar, and radiosondes during the LASE Validation Experiment, which was conducted in September 1995 near Wallops Island, Virginia, showed the LASE water vapor mixing ratio measurements to have an accuracy of better than 6% or 0.01 g/kg, whichever is larger, across the troposphere [Browell et al., 1997].

In addition to measuring water vapor mixing ratio, LASE also simultaneously measures aerosol backscattering at the off-line wavelength near 815 nm. Ismail et al. [1999] describe in detail the methods used to derive aerosol profiles using this off-line laser return signal, so only a brief description will be given here. Assuming a region with very low aerosol loading can be identified, profiles of the total scattering ratio, defined as the ratio of total (aerosol plus molecular) scattering to molecular scattering, are determined by normalizing the scattering in the region containing enhanced aerosol scattering to the expected scattering by the "clean" atmosphere at that altitude. In this "clean" region, typically located between 8 and 12 km, the total scattering ratio is assumed to be 1.05 at 815 nm based on the background aerosol loading conditions [Russell et al., 1979]. The aerosol backscatter coefficient is then computed from the total scattering ratio and the molecular backscattering cross section derived from radiosonde pressure and temperature profiles.

7. LASE Operations During TARFOX

During TARFOX, LASE was mounted in the Q-bay of the NASA ER-2 aircraft, and collected a total of 24 flight hours of

data over nine flights between July 14 and 26, 1996. The ER-2 normally flew at an altitude of about 19 km at a speed of about 200 m s⁻¹. The nominal averaging interval for the water vapor data was 3 min corresponding to a horizontal distance of about 36 km. The vertical resolution for the water vapor data varied with altitude, from 150 m for 0-1 km to 330 m for 1-10 km, and 510 m for 10-15 km. The LASE aerosol profiles, which span the altitude range between 0.03 and 18 km, typically have horizontal and vertical resolutions of 600 and 60 m, respectively.

The ER-2 flights during TARFOX were coordinated with overflights of the NOAA 14, ERS-2, and Landsat satellites, and with flights by the other TARFOX aircraft, including the University of Washington (UW) C-131A, the United Kingdom (UK) Meteorological Research Flight C-130, and the Center for Interdisciplinary Remotely Piloted Aircraft Studies (CIRPAS) Pelican. These flights occurred predominantly over the Atlantic Ocean 100-300 km east of Wallops Island, Virginia, although several flight legs were flown over surface sites at Wallops Island and other east coast sites. A complete description of TARFOX operations is given by Whiting et al. [1996] and Russell et al. [1999a], while Ismail et al. [this issue] give an overview of the LASE measurements during TARFOX.

8. LASE Measurements

Total scattering ratios were computed from the LASE off-line return wavelengths at 815 nm following the methods described by Ismail et al. [this issue]. Although water vapor absorption at this off-line wavelength is much weaker than at the on-line wavelength, it is still significant in the lowest part of the boundary layer. Neglecting water vapor absorption in this off-line wavelength would lead to 50-100% errors in the derived total scattering ratios for typical water vapor amounts observed during TARFOX. Therefore the LASE water vapor profiles were used in correcting for water vapor absorption.

The total scattering ratio profiles derived from the LASE data were also corrected for the attenuation produced by aerosols in the lower troposphere. An iterative technique was used to determine the total scattering ratio profile as well as an estimate of the aerosol extinction profile. Ismail et al. [this issue] describe this technique and show that it produces results equivalent to that produced by the Bernoulli inversion method [Fernald, 1984; Klett, 1981]. The retrieval of the total scattering ratio R requires estimates of the total scattering ratio in the "clean" region of the upper troposphere as well as an estimate of the aerosol extinction/backscattering ratio S_a . In this "clean" region, typically located between 8 and 12 km, the total scattering ratio is assumed to be 1.05 at 815 nm based on the background aerosol loading conditions [Russell et al., 1979]. The sensitivity of the derived total scattering ratio profile to this assumed value is small [Ismail et al., this issue]. A rather large overestimate of 0.05 in this assumed reference value produces an overestimate of only about 8-10% in the derived scattering ratio and aerosol extinction in the lowest kilometer and about a 10% change in the derived AOT.

The retrievals of atmospheric scattering ratio and aerosol extinction from the LASE measurements also require an estimate of S_a . For the LASE TARFOX analyses, a value of $S_a = 60$ sr was used on the basis of the retrieval of this value by the GSFC Raman lidar, as discussed in section 2. This same value was used for LASE, although the wavelength for LASE (815 nm) was different than that of the SRL (355 nm). S_a can either decrease

or increase with wavelength depending on the type of aerosol and the relative humidity [Evans, 1988; Whitlock et al., 1985; Takamura and Sasano, 1990; Ackerman, 1998]. Because of this uncertainty in the wavelength behavior of S_a we chose to use the same value ($S_a = 60$ sr) for the LASE aerosol retrievals as was used for the SRL analyses. While varying the aerosol extinction/backscatter ratio with both time and altitude would most likely improve the LASE aerosol extinction retrievals, without additional information from the Raman N_2 channel of the SRL, it is difficult to know the appropriate S_a value to use. Therefore a constant value of S_a was used for both the SRL and the LASE aerosol extinction retrievals throughout these analyses. The value of $S_a = 60$ sr (815 nm) is consistent with the values of $S_a = 60$ and 51 sr (at 815 nm) derived by Redemann et al. [this issue] for July 17 and July 24, respectively, using aerosol size distributions measured by in situ instrumentation on the University of Washington C-131A aircraft.

Ismail et al. [this issue] discuss the sensitivities of the LASE retrievals of total scattering ratio and extinction profiles to S_a . Decreasing S_a from 60 to 30 sr causes the total scattering ratio to decrease by about 15% in the lowest kilometer. However, this same 50% decrease in S_a causes the aerosol extinction to decrease by about 50% in the lowest kilometer and also causes the AOT to decrease by this same amount. Thus the aerosol extinction and AOT measurements derived from the LASE data were found to be nearly linearly related to changes in S_a , so uncertainty in the value of the aerosol extinction/backscattering ratio leads to large errors in the derived aerosol extinction profile and AOT. The sensitivity of the derived aerosol extinction coefficient profile and AOT is much greater than in the case of the SRL discussed in section 2. This difference is mostly due to the difference in the solution form between the lidar systems. In the first case of the SRL the solution represents the more stable case of the backward solution, where the reference value of the total scattering ratio (or aerosol extinction) is taken at the far end of

the lidar return signal and the integration proceeds toward the lidar. In the second case dealing with LASE aerosol retrievals, the integration procedure proceeds away from the reference value of total scattering ratio and the lidar. Klett [1981] has shown this forward solution is much more sensitive to errors in the reference value of total scattering ratio and aerosol extinction/backscattering ratio.

9. LASE and SRL Aerosol Profile Comparisons

The total scattering ratios measured by LASE over Wallops Island were compared with those measured by the SRL as shown in Figure 5. The lidar profiles were acquired within about 10 min of each other. Since LASE and the SRL measured aerosol profiles at different wavelengths, the LASE total scattering ratio profiles were scaled to 355 nm using the wavelength dependence of AOT between 340 nm and 1020 nm measured at Wallops Island by the ground-based Cimel Sun photometer. This wavelength dependence, which is expressed as the exponent α in the expression $\lambda^{-\alpha}$, varied between 1.0 and 1.7 during the 5 days of coincident LASE and SRL measurements. We estimate that the uncertainty introduced when using this technique to scale the LASE values to 355 nm is less than 10%. This uncertainty was estimated by using this technique to estimate AOT at 340 nm and comparing the resulting estimates to the measured AOT values at 340 nm.

The agreement between the total scattering ratios measured by both systems was good, even on July 20 and 21, when scattering ratios were quite low. The increase in noise shown in the LASE profile on July 20 was due to attenuation by cirrus clouds. The overall comparison between the scattering ratios measured by both lidar systems is shown in Figure 6. When compared to the SRL total scattering ratios, the LASE total scattering ratios, when scaled to 355 nm, have a bias difference (LASE-SRL) of 0.049 (4%) and a rms difference of 0.122 (11%). The generally good

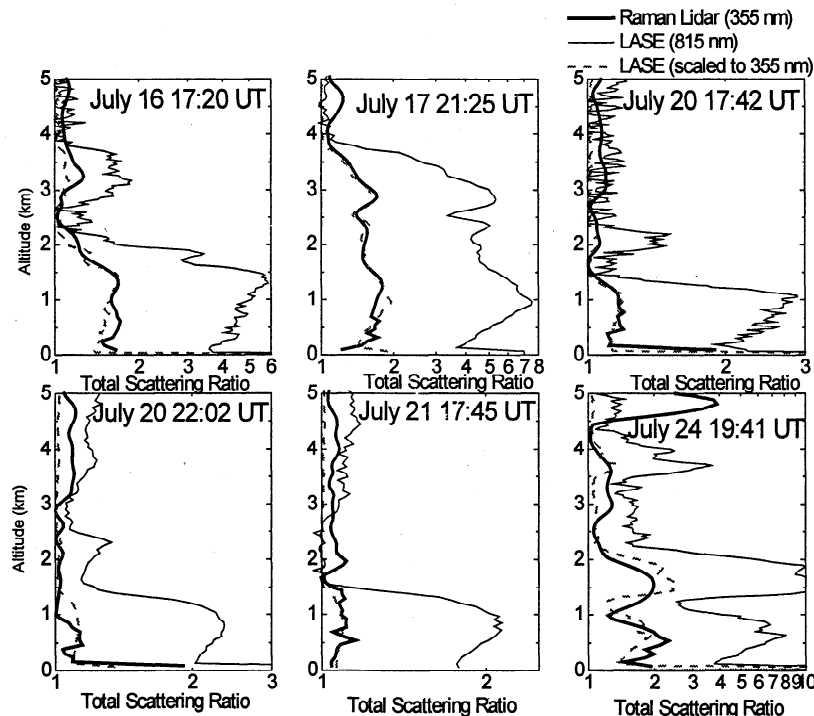


Figure 5. Comparison of total scattering ratio profiles measured by the GSFC lidar and by Lidar Atmospheric Sensing Experiment (LASE) during flights of the ER-2 over Wallops Island.

TARFOX July 1996 Comparison of Lidar Scattering Ratios

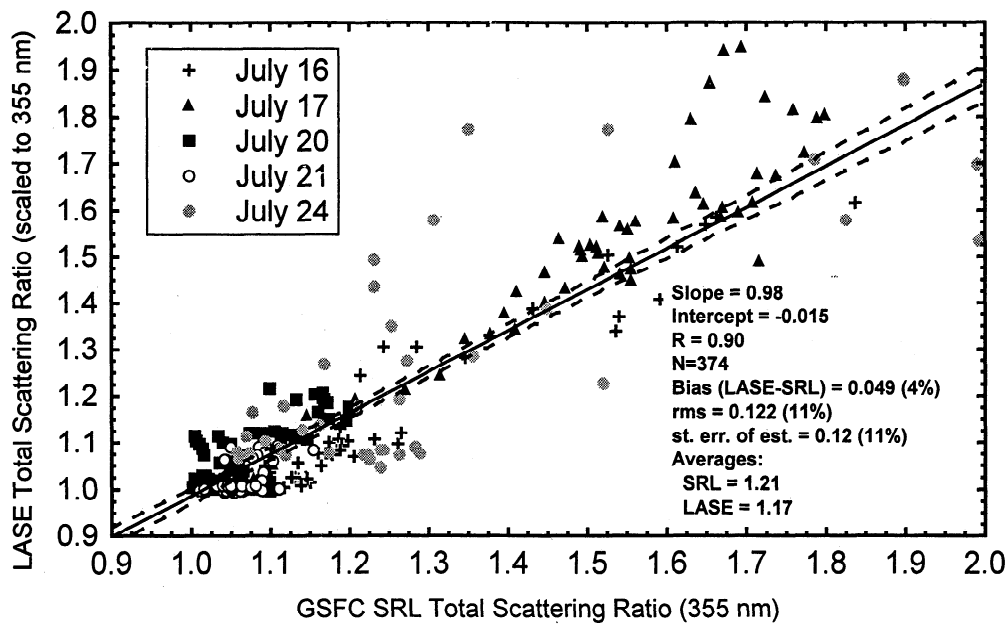


Figure 6. Comparison of total scattering ratios measured by the GSFC lidar and by LASE during TARFOX.

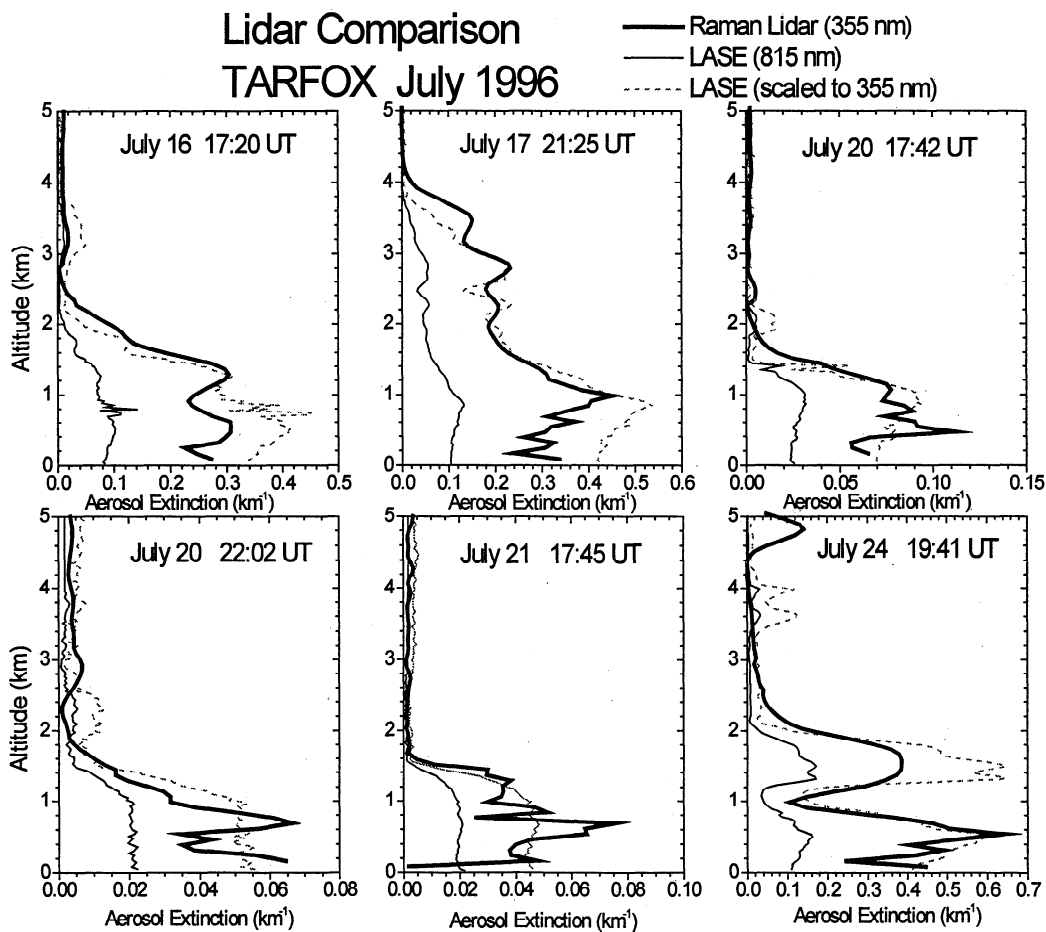


Figure 7. Comparison of aerosol extinction profiles measured by the GSFC lidar and by LASE during flights of the ER-2 over Wallops Island.

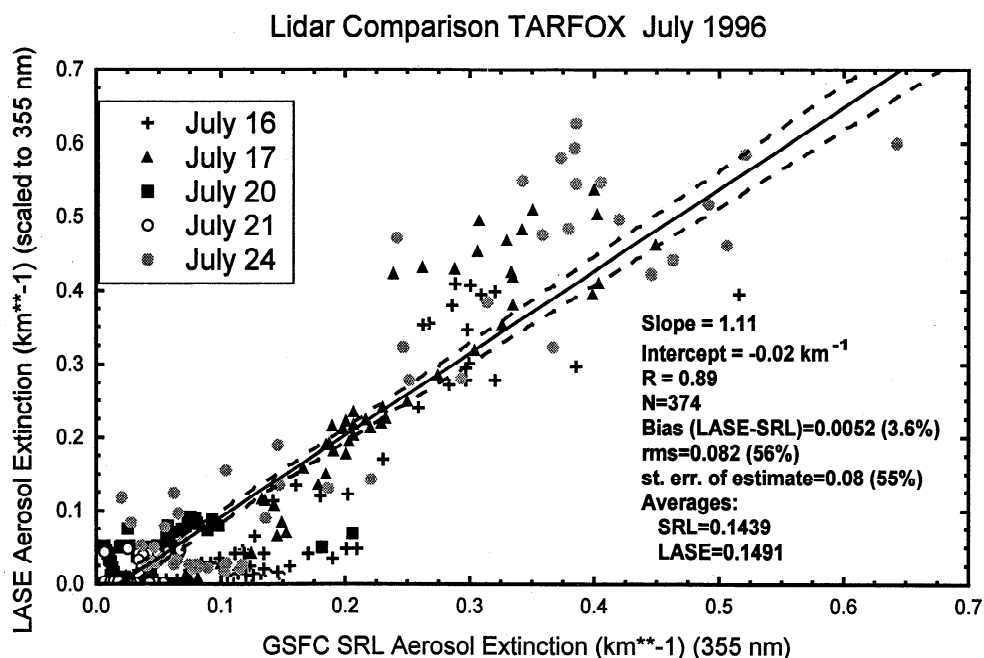


Figure 8. Comparison of aerosol extinction coefficients measured by the GSFC lidar and by LASE during TARFOX.

agreement between scattering ratio profiles indicates that aerosol backscattering, as well as aerosol extinction, generally scaled with the wavelength dependence of AOT.

Aerosol extinction coefficient profiles were computed from the LASE data for each flight. A comparison of the aerosol extinction profiles derived by LASE and the SRL is shown in Figure 7. The overall comparison between aerosol extinction coefficients measured by both lidars is shown in Figure 8. The wavelength dependence of AOT measured at the surface by the Cimel Sun photometer was used to scale the LASE aerosol extinction coefficient profiles to the SRL wavelength of 355 nm. In this case, the aerosol extinction profiles tend to show the same features, although the agreement is not quite as good as in the case of the total scattering ratio shown in Figure 6. When compared to the SRL aerosol extinction coefficients, the LASE aerosol extinction coefficients, scaled to 355 nm, have a bias difference (LASE-SRL) of 0.0052 km⁻¹ (3.6%) and a rms difference of 0.082 km⁻¹ (56%). On July 16, 17, and 24 the LASE aerosol extinction coefficient profiles, extrapolated to 355 nm, were greater than the SRL returns by over 50% in some altitude regions. These differences are most likely due to the choice of the aerosol extinction/backscattering S_a ratio used in the LASE aerosol retrieval algorithm. Since S_a depends on the aerosol size distribution, particle composition (i.e., refractive index), particle shape, and single-scattering albedo, it is unrealistic to expect that these aerosol properties would remain constant in both time and altitude during the TARFOX period. Previous measurements have shown that S_a varies with time and altitude [Ferrare *et al.*, 1998a]. Modeling studies, which use Mie theory to compute aerosol extinction and backscattering based on aerosol size and composition, have shown that S_a also can vary with relative humidity for hygroscopic particles since the particles grow and change composition with increasing relative humidity [Ackerman, 1998]. Such a variation in S_a with altitude may explain the difference in aerosol extinction profiles between the two lidar systems observed on July 24. Comparisons of the aero-

sol extinction profiles and aerosol optical thicknesses derived from both the SRL and LASE data with other in situ and remote sensing measurements of these aerosol parameters gives a quantitative indication of the limitations in using a single S_a value. These comparisons are discussed by Ferrare *et al.* [this issue].

10. LASE and Sun Photometer Aerosol Optical Thickness Comparisons

The LASE measurements of aerosol extinction coefficient profiles were integrated with altitude to derive AOT. Profiles of AOT were computed as a function of altitude for the LASE data by integrating the aerosol extinction profiles between the top of the profile (about 16 km) and each altitude. A comparison of these estimates of AOT with those measured by both the airborne (AATS 6) and the ground-based (Cimel) Sun photometers is shown in Figure 9. Airborne Sun photometer data that were within 30 m in altitude, 15 km in horizontal distance, and within about 6 min of the LASE measurements were selected for this comparison. The airborne Sun photometer data were logarithmically interpolated between 525 nm and 1021 nm to the LASE wavelength of 815 nm. Comparisons with the ground-based Sun photometers were performed when the ER-2 flew within about 20 km and 30 min of the Cimel measurements. Two of the Cimel Sun photometers were located on the Virginia coast, at Wallops Island (37.93°N, 75.46°W) and Cheriton (37.27°N, 75.42°W); a third was located at Bermuda (32.37°N, 64.68°W); and fourth was on the cruise ship *Meridian*. The data from the Cimel Sun photometer on the *Meridian* were used when the ship was located at 37.79°N, 70.54°W on July 20 and 32.39°N, 64.57°W on July 26. When compared with the AOT measured by the Cimel Sun photometers, the LASE AOT values have a bias difference (LASE-Cimel) of 0.0033 (3%) and a rms difference of 0.036 (34%). Only six points were used in this comparison because of the lack of ER-2 overflights of the ground-based Sun photometers during cloud-free conditions. When compared with the much

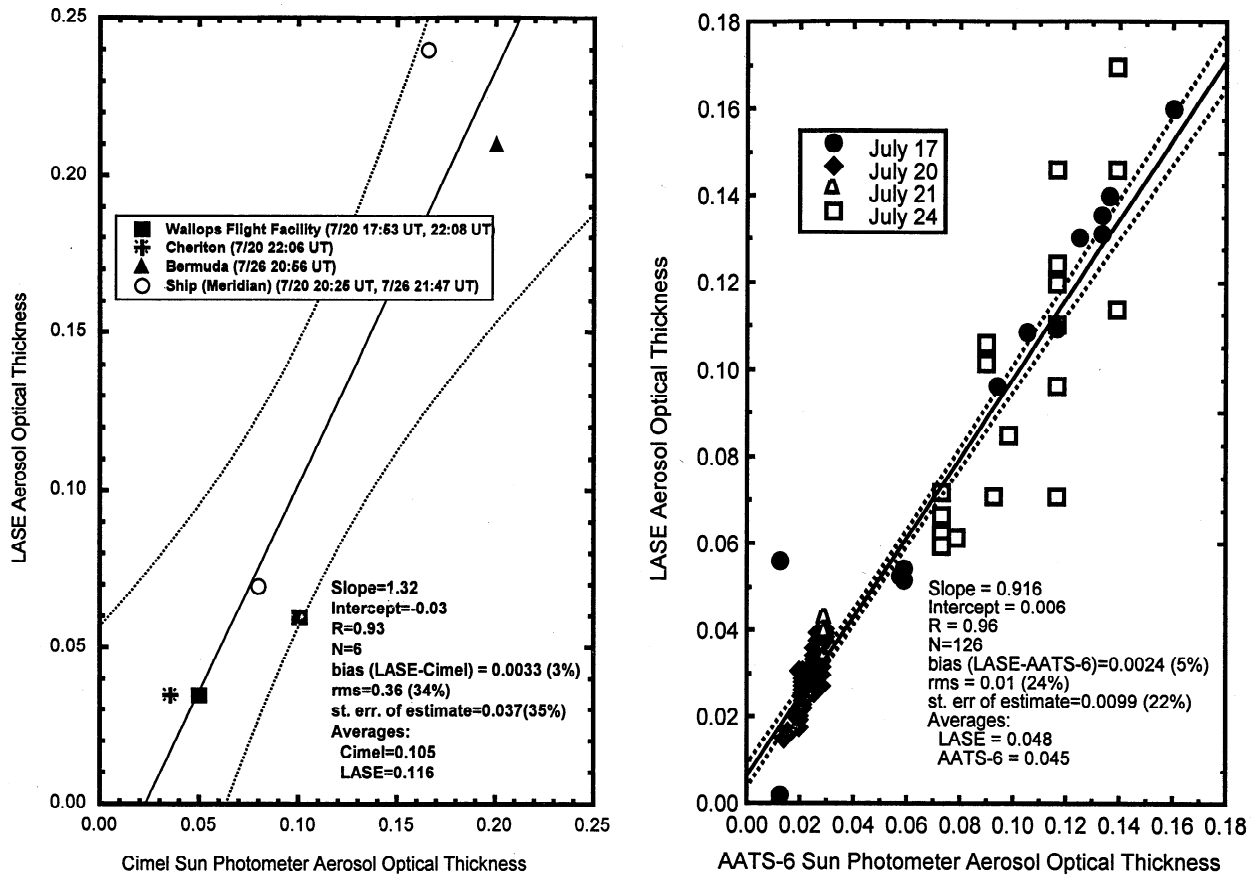


Figure 9. (left) Comparison of AOT (815 nm) measured by LASE and Cimel Sun photometer during TARFOX. (right) Same except for AATS-6 airborne Sun photometer flown on the UW C-131A aircraft.

larger airborne Sun photometer data set, the AOT measured by LASE had a bias difference (LASE-Sun photometer) of 0.002 (5%) and a rms difference of 0.01 (24%). This rms difference on this airborne Sun photometer AOT comparison is higher than the 10% rms difference on the precipitable water vapor comparison discussed in the next section. This AOT difference did not vary appreciably as a function of altitude. These differences are most likely due to the temporal and spatial variations in the aerosol extinction/backscattering ratio as well as spatial variations in the aerosol scattering and extinction observed by both sensors. However, this figure does show that at least for the retrieval of AOT as a function of altitude during TARFOX, a single value of $S_a = 60$ sr can be used to estimate AOT to within about 25%. The overall 5-10% high bias of the LASE measurements also suggests that the most appropriate single, constant S_a value should most likely be in the range of 55-57 sr, which is within the range of 60 sr (July 17) and 51 sr (July 24) obtained by Redemann *et al.* [this issue] for measurements acquired during TARFOX.

11. LASE and Sun Photometer Precipitable Water Vapor Comparisons

Precipitable water vapor (PWV) was estimated by integrating the LASE water vapor mixing ratio measurements with altitude. For the purposes of estimating PWV the water vapor mixing ratio was assumed to be constant between the surface and the minimum altitude of the LASE measurements, which was between

0.2 and 0.3 km during TARFOX. To compute total PWV, the LASE water vapor measurements were integrated to a maximum altitude of about 14 km during cloud-free periods. PWV was also computed as a function of altitude from the LASE data and was compared with the PWV derived from the airborne Sun photometer measurements on the C-131A. PWV was derived from the AATS-6 instrument using a model approach as described by Schmid *et al.* [1996]. The comparison between LASE and airborne Sun photometer PWV is shown in Figure 10. The temporal difference between the LASE and the Sun photometer measurements was less than 6 min, while the vertical and horizontal distances were less than 30 m and 15 km, respectively. The two measurements of water vapor are in good agreement, with the airborne Sun photometer estimates only slightly (~5-10%) higher than those from LASE. This uncertainty may be due in part to the uncertainty in the Sun photometer calibration constant and model, LASE water vapor measurements, and/or the uncertainty in the water vapor mixing ratio profile below 300 m.

12. Lidar Measurements of Cloud, Aerosol, and Water Vapor Distributions

Data from both lidars were used to identify cloudy periods and the cloud altitudes. Figure 11 shows histograms of cloud base altitudes derived from the SRL measurements; cloud bases are grouped into 1-km-wide bins for each day of observations. The percentages of observations that had cloud bases at each altitude are also shown. These results show only the base of the lowest

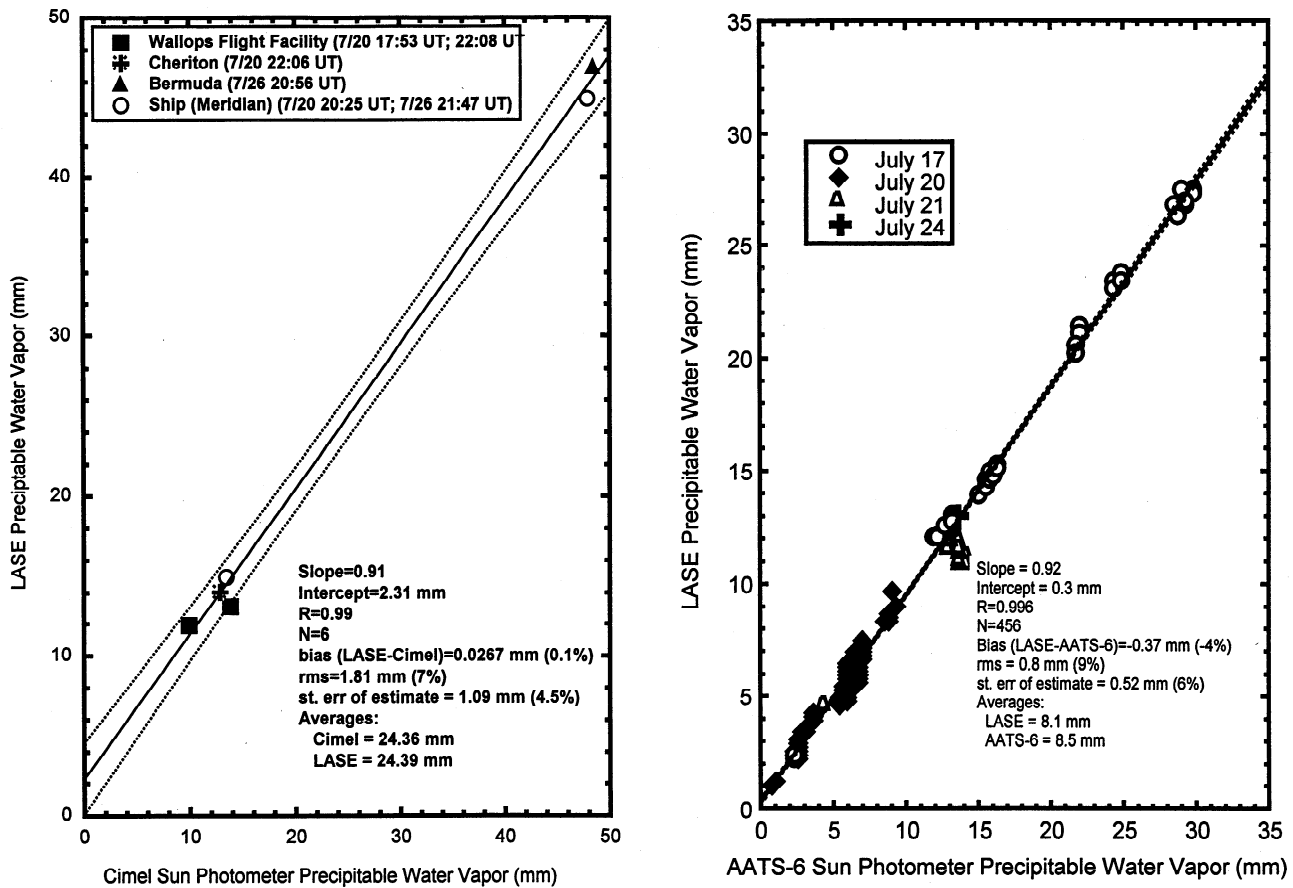


Figure 10. (left) Comparison of precipitable water vapor (PWV) measured by LASE and Cimel Sun photometer during TARFOX. (right) Same except for AATS-6 airborne Sun photometer flown on the UW C-131A aircraft.

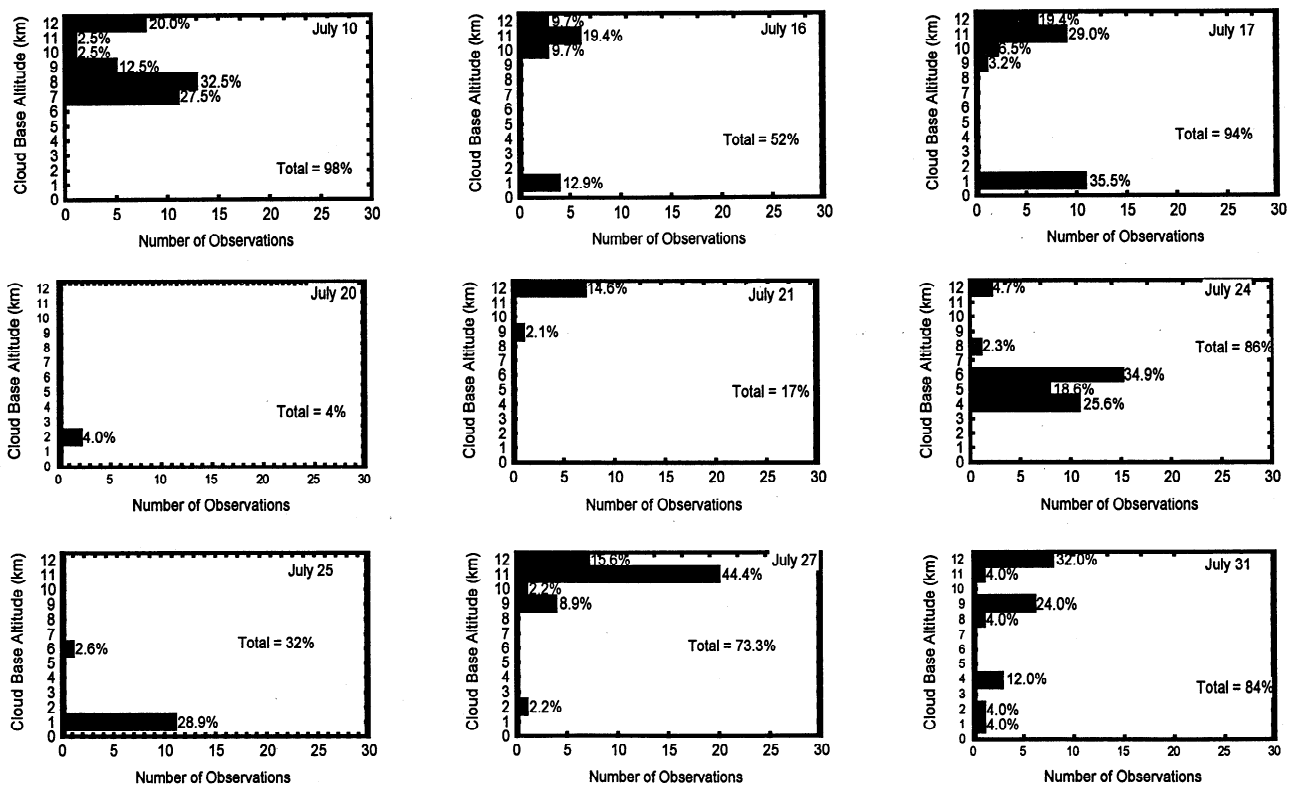


Figure 11. Distributions of cloud base altitudes measured by the GSFC lidar during TARFOX. The total percentage of observations which observed clouds is listed for each day.

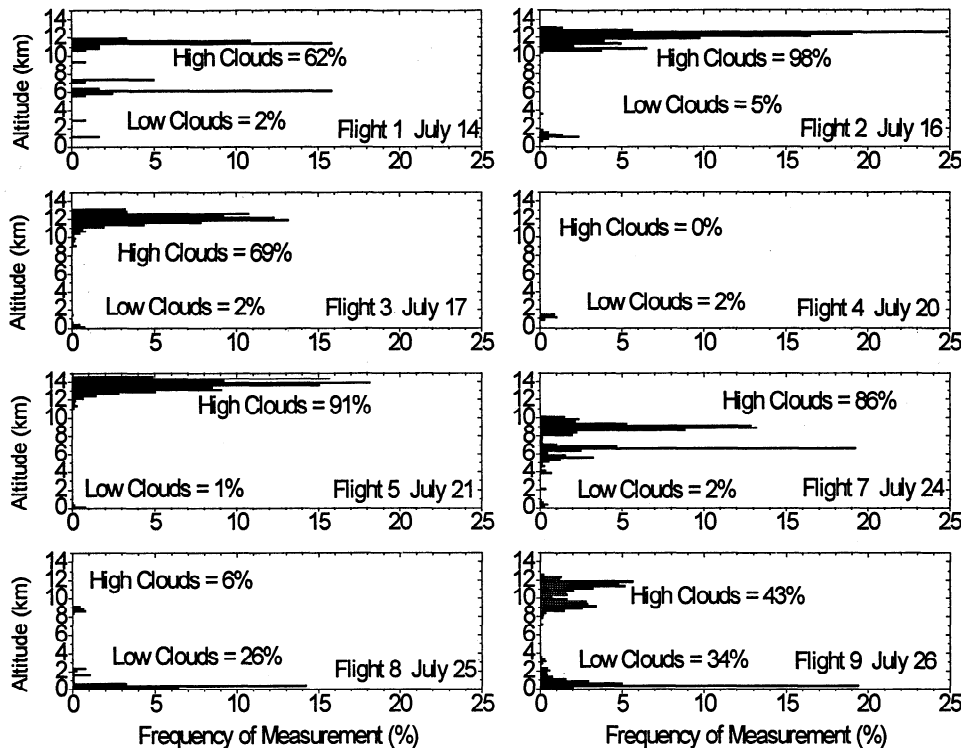


Figure 12. Distributions of cloud top altitudes measured by LASE during TARFOX. The total percentage of observations which observed both high (>4 km) and low (<4 km) clouds is listed for each day.

cloud layer and do not show the presence of multiple cloud layers. In addition, no attempt was made to determine the optical thickness of these clouds. It is interesting to note that even though lidar and TARFOX operations tended to be conducted during clear daytime periods, the lidar still observed clouds during about two thirds of the time during these operations. This frequent occurrence of clouds often limited the opportunities to coordinate ground, aircraft, and satellite measurements of aerosol properties.

Clouds were also identified using the atmospheric scattering ratios measured by LASE. High clouds, which were designated as clouds above 4 km, were defined to be present when the scattering ratios (815 nm) were greater than 10. Clouds below 4 km were designated low clouds and were defined to be present when scattering ratios (815 nm) exceeded 30. The frequency of occurrence of both high and low clouds are shown as a function of altitude in Figure 12. The frequencies shown in this figure represent the percentages of the total LASE measurement time that cloud tops were observed in each of the 250-m-wide vertical bins during each flight. Note that a given profile may have contained multiple layers of clouds both above and below 4 km. In such a case, only the altitude of the cloud top of the highest layer is represented in Figure 12. The LASE observations of cloud top altitudes, like the GSFC ground-based lidar measurements of cloud bases, indicated high frequencies of high clouds above 8–10 km. Both lidar systems show that clouds were present within the TARFOX observational area during most of the observational periods. The relatively high occurrence of low clouds observed on July 26 is also consistent with the high relative humidity observed by LASE in the lowest 500 m, as discussed by Ferrare *et al.* [this issue].

The average vertical distribution of aerosols above Wallops Island during TARFOX was estimated by averaging the SRL and LASE measurements. Figure 13 (bottom axes) shows the average aerosol extinction profiles for each of the nine days of the SRL measurements. The average AOT profiles derived from these aerosol extinction measurements are also shown in Figure 13 (top axes). The AOT profiles represent the AOT, between 0 and 5 km, above each altitude. While most of the aerosols were concentrated near the surface as expected, elevated aerosol layers were observed on several days, including July 10, 16, 17 (recall Plate 1 and Figure 5), 24, and 27.

The LASE water vapor and aerosol measurements were used to produce average water vapor and aerosol profiles during each flight. To reduce possible low-cloud contamination, these profiles were constructed using all cloud-free profiles acquired by LASE on these days. The LASE profiles that did not contain low or high clouds below 6 km were used to compute the average aerosol and water vapor profiles. Average water vapor profiles, in terms of both water vapor mixing ratio and precipitable water vapor, are shown in Figure 14, while the corresponding aerosol profiles, in terms of both aerosol extinction and aerosol optical thickness, are shown in Figure 15. Error bars represent the standard deviations of the measurements. Because of the large variability in aerosol and water vapor distributions in the TARFOX region, these profiles are not meant to represent “average” distributions, but rather to show the day-to-day variability in both aerosols and water vapor distributions in the TARFOX area. These profiles show, as expected, correlations between aerosol and water vapor amounts, with July 20 and 21 having generally dry and clean conditions and July 24 and 26 having generally wetter and hazy conditions. Since the aerosol scattering meas-

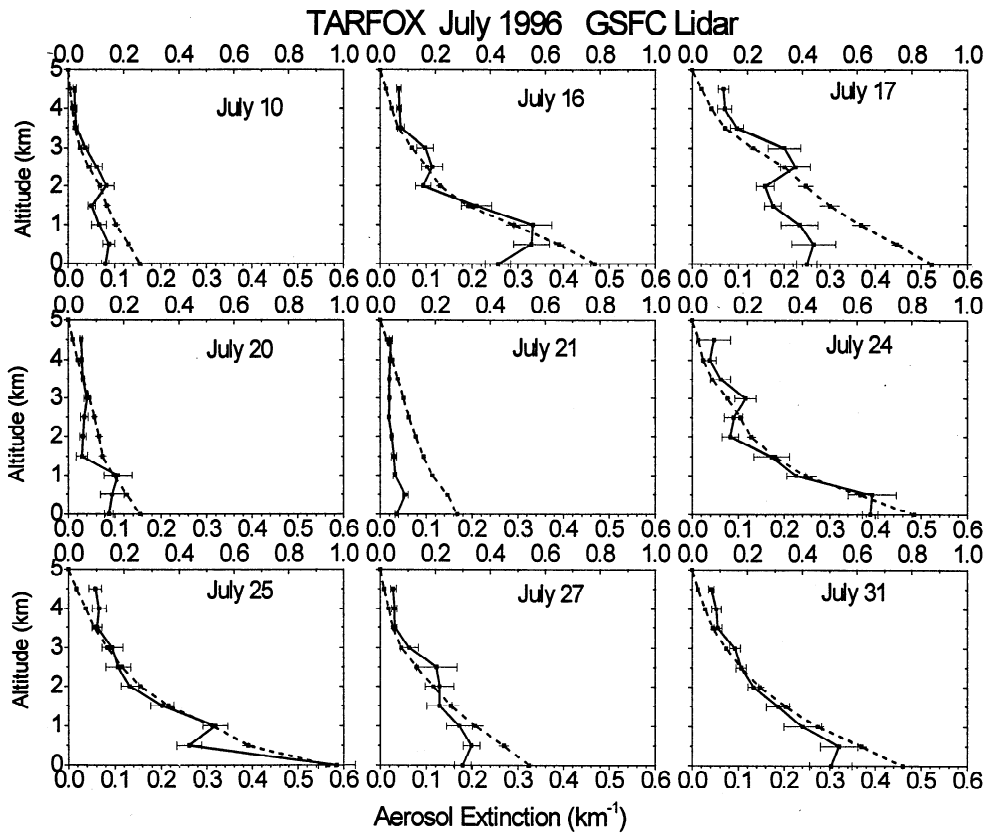


Figure 13. Average aerosol extinction (solid lines, bottom axes) and aerosol optical thickness profiles (dashed lines, top axes) measured by the GSFC lidar during each day during TARFOX.

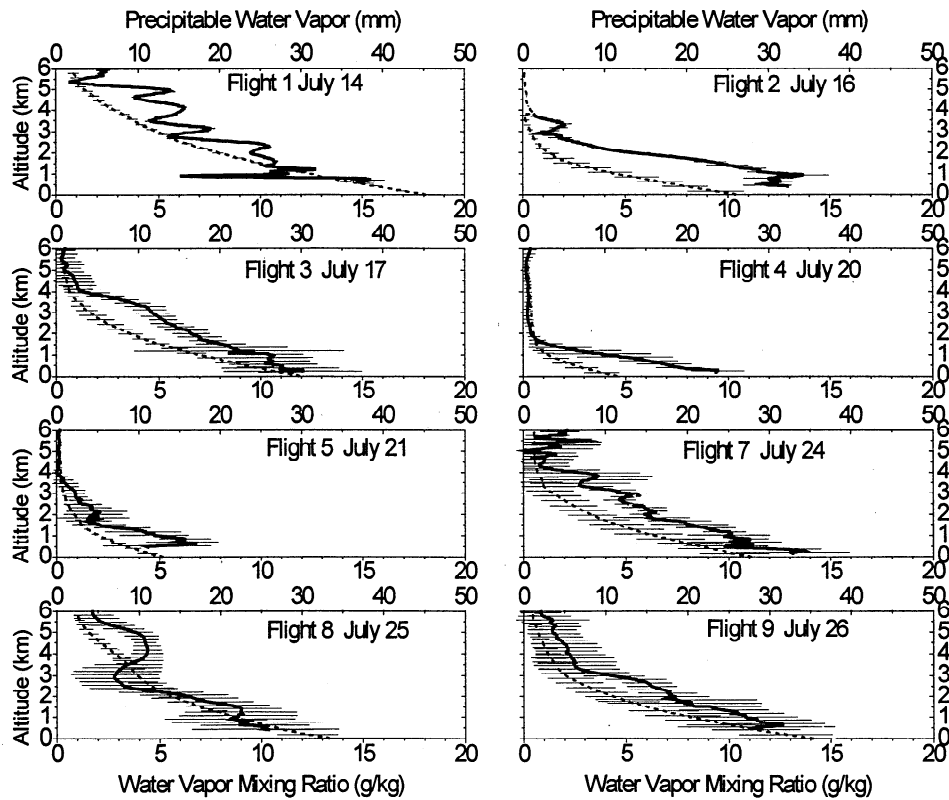


Figure 14. Average water vapor mixing ratio (solid lines, bottom axes) and precipitable water vapor profiles (dashed lines, top axes) measured by LASE during ER-2 flights at TARFOX.

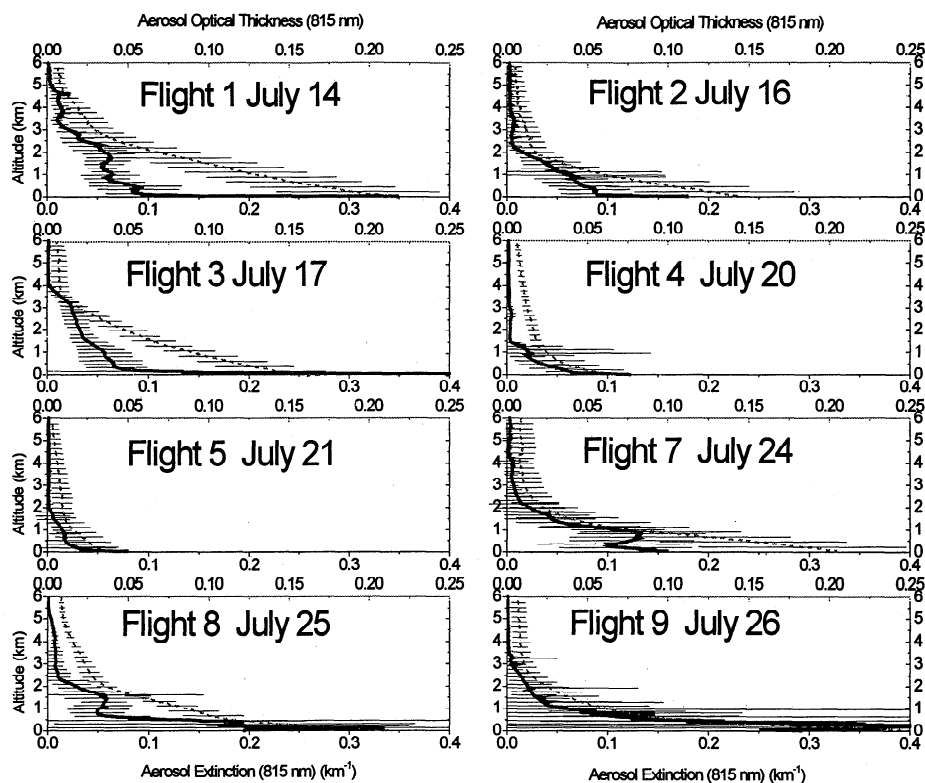


Figure 15. Average aerosol extinction (solid lines, bottom axes) and aerosol optical thickness profiles (dashed lines, top axes) measured by LASE during ER-2 flights at TARFOX.

ured during TARFOX was found to be highly dependent on water vapor [Hegg *et al.*, 1997; Kotchenruther *et al.*, 1999], the strong correlation between the AOT and the PWV profiles is not unexpected. In general, 90% of AOT and PWV were located below 3–3.5 km.

13. Conclusions

We have performed an “external” closure study using ground and airborne lidar and Sun photometer measurements acquired during the TARFOX experiment near the east coast of the United States. Measurements of aerosol backscattering and extinction from the ground-based GSFC scanning Raman lidar, which was located at Wallops Island, Virginia, were used to derive a value of $S_a = 60$ sr on July 27, 1998, for the aerosol extinction/backscattering ratio at 355 nm. Because of increased background skylight in the Raman nitrogen channels during daytime operations, aerosol extinction profiles and aerosol optical thickness (AOT) were derived from the SRL by inverting the data acquired at the laser wavelength using the S_a value above. The resulting AOT derived from this lidar were generally about 10% higher than the AOT measured by a ground-based Cimel Sun photometer and the airborne AATS-6 Sun photometer flown on the University of Washington C-131A aircraft.

The Lidar Atmospheric Sensing Experiment (LASE) flew on the NASA ER-2 and measured aerosol and water vapor profiles during TARFOX. Total scattering ratio profiles measured at 815 nm by LASE, when scaled to the SRL wavelength of 355 using the multiple-wavelength Sun photometer measurements of AOT, had a bias differences (LASE-SRL) of 0.049 (4%) and a rms difference of 0.122 (11%) when compared to the SRL total

scattering ratios. Similar comparisons between the aerosol extinction coefficients derived from the SRL measurements at 355 nm, and the LASE measurements at 815 nm and scaled to the SRL wavelength of 355 nm, showed a bias difference of 0.0052 (3.6%) and a rms difference of 0.082 (56%). Estimates of AOT obtained by integrating the LASE aerosol extinction profiles were compared with AOT measured by an airborne Sun photometer and were found to have a bias difference of 0.0024 (5%) and a rms difference of 0.01 (24%).

The relatively good agreement between the lidar estimates of AOT and the Sun photometer measurements suggests that an appropriate value of the lidar aerosol extinction/backscatter ratio for this experiment is between 55 and 60 sr. This value is in the range of values expected for a “continental” aerosol, as described by Ackermann [1998]. The fact that a single value of S_a could be used to derive AOT from the lidar measurements and achieve good agreement with Sun photometer measurements is somewhat surprising because of the dependence of S_a on the physical characteristics of the aerosols (i.e., size and composition). In the case of hygroscopic aerosols such as those observed during TARFOX [Kotchenruther *et al.*, 1999], changes in these aerosol physical characteristics caused by variations in relative humidity affect aerosol size and composition and in turn vary S_a . However, as shown in Figure 2, AOT values derived from the SRL in this study are not very sensitive to S_a ; this may explain the success in using a single value of S_a . Ferrare *et al.* [this issue] show also that the aerosol extinction profiles derived from the LASE data, in addition to the AOT estimates, are in reasonable agreement with profiles derived from the airborne in situ and Sun photometer data. However, during certain periods the lidar and Sun photometer measurements of AOT differed significantly, possibly

because of variations in the aerosol physical characteristics (e.g., size, composition) which affect S_a .

These comparisons indicate that ground and airborne lidar systems can be used to estimate aerosol extinction and optical thickness profiles for use in climate and radiation studies. However, it is important to have additional information regarding the relationship between aerosol extinction and backscattering for these retrievals to be valid. Such information can be provided using Raman-scattering channels, as done here, or by constraining the lidar retrievals using AOT measured by another sensor, such as a ground or airborne Sun photometer. This latter approach will be important for space-based lidar systems under development and can enable these systems to provide valuable information to assess the impact of aerosols on radiation and climate. It will be important to use ground and airborne Sun photometer AOT measurements to assess these future space-based lidar aerosol profiles.

LASE also measured profiles of water vapor mixing ratios which were then integrated to provide estimates of the precipitable water vapor (PWV). These PWV measurements were compared to PWV derived from the AATS-6 Sun photometer measurements acquired from the C-131A aircraft. The PWV derived from both systems were in good agreement as the Sun photometer measurements were only about 5-10% higher than those measured using LASE.

Both lidar systems were used to identify the presence of clouds and to determine the "average" altitude distributions of aerosols. Although TARFOX operations were preferentially selected to occur during cloud-free periods, the SRL observed clouds during two thirds of the operating time. Cloud bases for these clouds were generally observed above 9 km. Similarly, the LASE observations from the ER-2 observed clouds during about half of the operations even though flight tracks were generally selected to avoid cloudy regions. Nearly 90% of the cloud tops observed by LASE were above 6 km. Measurements from both lidar systems indicated that 90% of the aerosol extinction and AOT were located below 3.5 km. The LASE measurements also indicated that about 90% of the water vapor mixing ratio and PWV were also located below this altitude.

Acknowledgments. This research was conducted as part of the Tropospheric Aerosol Radiative Forcing Observational Experiment (TARFOX), which is a contribution to the International Global Atmospheric Chemistry (IGAC) core project of the International Geosphere-Biosphere Programme (IGBP). Financial support for the measurements and analyses was provided by the U.S. National Aeronautics and Space Administration, National Science Foundation, Office of Naval Research, Department of Energy, National Oceanographic and Atmospheric Administration, U.K. Meteorological Office, French Science Foundation (Centre National de la Recherche Scientifique (CNRS)), and the French Space Administration (Centre National d'Etudes Spatiales (CNES)). Special thanks are extended to the NASA Wallops Flight Facility, which provided many facilities and personnel to support the TARFOX IFC.

References

- Ackermann, J., The extinction-to-backscatter ratio of tropospheric aerosol: A numerical study, *J. Atmos. Oceanic Technol.*, **15**, 1043-1050, 1998.
- Ansmann, A., M. Riebesell, and C. Weitkamp, Measurement of atmospheric aerosol extinction profiles with a Raman lidar, *Opt. Lett.*, **15**, 746-748, 1990.
- Ansmann, A., M. Riebesell, U. Wandinger, C. Weitkamp, E. Voss, W. Lahmann, and W. Michaelis, Combined Raman elastic-backscatter LIDAR for vertical profiling of moisture, aerosol extinction, backscatter, and LIDAR ratio, *Appl. Phys. Ser. B*, **55**, 18-28, 1992.
- Browell, E. V., and S. Ismail, First lidar measurements of water vapor and aerosols from a high-altitude aircraft, *OSA Opt. Remote Sens. Atmos. Tech. Dig.*, **2**, 212-214, 1995.
- Browell, E. V., et al., LASE validation experiment, in *Advances in Atmospheric Remote Sensing with Lidar*, edited by A. Ansmann, R. Neuber, P. Rairoux, and U. Wandinger, pp. 289-295, Springer-Verlag, New York, 1997.
- Charlson, R. J., S. E. Schwartz, J. M. Hales, R. D. Cess, J. A. Coakley Jr., J. E. Hansen, and D. J. Hofmann, Climate forcing by anthropogenic aerosols, *Science*, **255**, 423-430, 1992.
- Demoz, B., K. F. Evans, M. Cadirola, S. H. Melfi, D. Starr, D. N. Whiteman, G. Schwemmer, and D. D. Turner, Determination of cloud base heights using the GSFC Raman lidar, *Proc. ARM Sci. Team Meet.*, **9**, 1999, http://www.arm.gov/docs/documents/technical/conf_9903/index.html, DOE ARM Experiment Center, Richland, WA.
- Evans, B. T. N., Sensitivity of the backscatter/extinction ratio to changes in aerosol properties: Implications for lidar, *Appl. Opt.*, **27**, 3299-3305, 1988.
- Fernald, F. G., Analysis of atmospheric lidar observations: Some comments, *Appl. Opt.*, **23**, 652-653, 1984.
- Ferrare, R. A., S. H. Melfi, D. N. Whiteman, and K. D. Evans, Raman lidar measurements of Pinatubo aerosols over southeastern Kansas during November-December 1991, *Geophys. Res. Lett.*, **19**, (15), 1599-1602, 1992.
- Ferrare, R. A., S. H. Melfi, D. N. Whiteman, K. D. Evans, F. J. Schmidlin and D. O'C. Starr, A comparison of water vapor measurements made by Raman lidar and radiosondes, *J. Atmos. Oceanic Technol.*, **12**, 1177-1195, 1995.
- Ferrare, R. A., S. H. Melfi, D. N. Whiteman, K. D. Evans, R. Leifer, and Y. J. Kaufman, Raman lidar measurements of aerosol extinction and backscattering, part 1, Methods and comparisons, *J. Geophys. Res.*, **103**, 19,663-19,672, 1998a.
- Ferrare, R. A., S. H. Melfi, D. N. Whiteman, K. D. Evans, M. Poellot, and Y. J. Kaufman, Raman lidar measurements of aerosol extinction and backscattering, part 2, Derivation of aerosol real refractive index, single scattering albedo, and humidification factor using Raman lidar and aircraft size distribution measurements, *J. Geophys. Res.*, **103**, 19,673-19,689, 1998b.
- Ferrare, R. A., et al., Comparisons of LASE, aircraft, and satellite measurements of aerosol optical properties and water vapor during TARFOX, *J. Geophys. Res.*, this issue.
- Hansen, J., M. Sato, and R. Ruedy, Radiative forcing and climate response, *J. Geophys. Res.*, **102**, 6831-6864, 1997.
- Hegg, D. A., J. Livingston, P. V. Hobbs, T. Novakov, and P. B. Russell, Chemical apportionment of aerosol column optical depth off the mid-Atlantic coast of the United States, *J. Geophys. Res.*, **102**, 25,293-25,303, 1997.
- Hobbs, P. V., An overview of the University of Washington airborne measurements and results from the Tropospheric Aerosol Radiative Forcing Observational Experiment (TARFOX), *J. Geophys. Res.*, **104**, 2233-2238, 1999.
- Holben, B. N., T. F. Eck, I. Slutsker, D. Tanre, J. P. Buis, A. Setzer, E. Vermote, J. A. Reagan, and Y. J. Kaufman, Multi-band automatic sun and sky scanning radiometer for measurement of aerosols, *Proc. Int. Symp. Phys. Meas. Signatures Remote Sens.*, **6**, 75-83, 1994.
- Holben, B. N., et al., AERONET—A Federated Instrument Network and data archive for aerosol characterization, *Remote Sens. Environ.*, **66**, 1-16, 1998.
- Intergovernmental Panel on Climate Change (IPCC), Radiative forcing of climate change, in *Climate Change*, edited by J. T. Houghton, L. G. Filho, J. Bruce, H. Lee, B. A. Callendar, E. Haites, N. Harris, A. Kattenberg, and K. Maskell, pp. 1-231, Cambridge Univ. Press, New York, 1995.
- IPCC, *Climate Change 1995: The Science of Climate Change*, edited by J. T. Houghton, L. G. Meira Filho, B. A. Callendar, N. Harris, A. Kattenberg, and K. Maskell, 572 pp., Cambridge Univ. Press, New York, 1996.
- Ismail, S., E. V. Browell, R. Ferrare, S. A. Kooi, M. Clayton, and V. Brackett, LASE measurement of aerosol and water vapor profiles measured during TARFOX, *J. Geophys. Res.*, this issue.
- Jager, H., T. Deshler, F. Homburg, and V. Freudenthaler, Five years of lidar observations of the Pinatubo eruption cloud, in *Advances in Atmospheric Remote Sensing With Lidar*, pp. 485-488, Springer-Verlag, New York, 1997.
- Kiehl, J. T., and B. P. Briegleb, The relative roles of sulfate aerosols and greenhouse gases in climate forcing, *Science*, **260**, 311-314, 1993.
- King, M. D., Y. J. Kaufman, W. P. Menzel, D. Tanre, and B. C. Gao,

- MODIS atmosphere validation plan, http://modarch.gsfc.nasa.gov/MODIS/ATBD/atm_val.pdf, 48 pp., NASA/Goddard Space Flight Center, Greenbelt, MD, 1999.
- Klett, J. D. Stable analytical inversion solution for processing lidar returns, *Appl. Opt.*, **20**, 211-220, 1981.
- Kotchenruther, R. A., P. V. Hobbs, and D. A. Hegg, Humidification factors for atmospheric aerosols off the mid-Atlantic coast of the United States, *J. Geophys. Res.*, **104**, 2239-2252, 1999.
- Kunz, G. J., and G. de Leeuw, Inversion of lidar signals with the slope method, *Appl. Opt.*, **32**, 3249-3255, 1993.
- Matsumoto, T., P. B. Russell, C. Mina, and W. Van Ark, Airborne tracking sunphotometer, *J. Atmos. Oceanic Technol.*, **4**, 336-339, 1987.
- Moore, A. S., Jr., et al., Development of the Lidar Atmospheric Sensing Experiment (LASE), an advanced airborne DIAL instrument, in *Advances in Atmospheric Remote Sensing With Lidar*, edited by A. Ansmann, R. Neuber, P. Rairoux, and U. Wandinger, pp. 281-288, Springer-Verlag, 1997.
- Redemann, J. P., et al., Retrieving the vertical structure of the aerosol complex index of refraction from aerosol in situ and remote sensing measurements during TARFOX, *J. Geophys. Res.*, this issue.
- Remer, L., S. Gasso, D. Hegg, Y. Kaufman, and B. Holben, Urban/industrial aerosol: Ground-based Sun/sky radiometer and airborne in situ measurements, *J. Geophys. Res.*, **102**, 16,849-16,859, 1997.
- Remer, L. A., Y. J. Kaufman, and B. N. Holben, Interannual variation of ambient aerosol characteristics on the east coast of the United States, *J. Geophys. Res.*, **104**, 2223-2231, 1999.
- Russell, P. B., T. J. Swisler, and M. P. McCormick, Methodology for error analysis and simulation of lidar measurements, *Appl. Opt.*, **18**, 3783-3797, 1979.
- Russell, P. B., et al., Pinatubo and pre-Pinatubo optical depth spectra: Mauna Loa measurements, comparisons, inferred particle size distributions, radiative effects, and relationship to lidar data, *J. Geophys. Res.*, **98**, 22,969-22,985, 1993.
- Russell, P. B., P. V. Hobbs, and L. L. Stowe, Aerosol properties and radiative effects in the U.S. east coast haze plume: An overview of the Tropospheric Aerosol Radiative Forcing Observational Experiment (TARFOX), *J. Geophys. Res.*, **104**, 2213-2222, 1999a.
- Russell, P. B., J. M. Livingston, P. Hignett, S. Kinne, J. Wong, A. Chien, R. Bergstrom, P. Durkee, and P. V. Hobbs, Aerosol-induced radiative flux changes off the United States mid-Atlantic coast: Comparison of values calculated from Sun photometer and in situ data with those measured by airborne pyranometer, *J. Geophys. Res.*, **104**, 2289-2307, 1999b.
- Schmid, B., K. J. Thome, P. Demoulin, R. Peter, C. Mätzler, and J. Sekler, Comparison of modeled and empirical approaches for retrieving columnar water vapor from solar transmittance measurements in the 0.94 μm region, *J. Geophys. Res.*, **101**, 9345-9358, 1996.
- Schwartz, S., and M. O. Andreae, Uncertainty in Climate Change Caused by Aerosols, *Science*, **272**, 1121-1122, 1996.
- Smirnov, A., B. N. Holben, O. Dubovik, N. T. O'Neill, L. A. Remer, T. F. Eck, I. Slutsker, and D. Savoie, Measurement of atmospheric optical parameters on U.S. Atlantic coast sites, ships, and Bermuda during TARFOX, *J. Geophys. Res.*, this issue.
- Takamura, T., and Y. Sasano, Aerosol optical properties inferred from simultaneous lidar, aerosol-counter, and sunphotometer measurements, *J. Meteorol. Soc. Jpn.*, **68**, (6), 729-739, 1990.
- Whiteman, D., S. H. Melfi, and R. A. Ferrare, Raman lidar system for the measurement of water vapor and aerosols in the Earth's atmosphere, *Appl. Opt.*, **31**, (16), 3068-3082, 1992.
- Whiteman, D. N., et al., Comparison of measurements by the NASA/GSFC scanning Raman lidar and the DOE/ARM CART Raman lidar, in *Eighth ARM Science Team Meeting*, Dep. Of Energy, Tucson, Arizona, 809-812, March 23-27, 1998.
- Whiting, W., P. B. Russell, P. V. Hobbs, and L. L. Stowe, *TARFOX Operations Summary*, 140 pp., NASA Ames Res. Cent., Moffett Field, Calif., 1996.
- Whitlock, C. H., J. T. Suttles, and S. R. LeCroy, Phase function, backscatter, extinction, and absorption for standard radiation atmosphere and El Chichon aerosol models at visible and near-infrared wavelengths, *NASA Tech. Memo.* 86379, 1985.
- E. Browell, R. Ferrare, and S. Ismail, NASA Langley Research Center, Mail Stop 401A, Hampton, VA 23681-0001. (r.ferrare@larc.nasa.gov)
- V. Brackett, M. Clayton, and S. Kooi, SAIC/NASA Langley Research Center, Hampton, VA 23681-0001.
- K. Evans and S. H. Melfi, University of Maryland Baltimore County, Baltimore, MD 21250.
- B. Holben, L. Remer, G. Schwemmer, and D. Whiteman, NASA Goddard Space Flight Center, Greenbelt, MD 20771.
- P. Russell, NASA Ames Research Center, Moffett Field, CA 94035.
- J. Livingston, SRI International, Menlo Park, CA 94025.
- B. Schmid, BAER Institute, San Francisco, CA 94035.
- A. Smirnov, SSAI/NASA Goddard Space Flight Center, Greenbelt, MD 20771.
- P. V. Hobbs, Department of Atmospheric Science, University of Washington, Seattle, WA 98195.

(Received May 7, 1999; revised September 14, 1999; accepted November 19, 1999.)